Journal of Magnetic Resonance 195 (2008) 103–111

Contents lists available at ScienceDirect

Journal of Magnetic Resonance

journal homepage: www.elsevier.com/locate/jmr

Extensive NMRD studies of Ni(II) salt solutions in water and water–glycerol mixtures

J. Kowalewski [a,*], A. Egorov [b], D. Kruk [c], A. Laaksonen [a], S. Nikkhou Aski [a], G. Parigi [d], P.-O. Westlund [e]

[a] Department of Physical, Inorganic and Structural Chemistry, Stockholm University, Arrhenius Laboratory, S-106 91 Stockholm, Sweden
[b] Department of Physics, St. Petersburg State University, Russia
[c] Institute of Physics, Jagiellonian University, Reymonta 4, 30-059 Krakow, Poland
[d] Magnetic Resonance Center (CERM) and Department of Agricultural Biotechnology, University of Florence, I-50144 Florence, Italy
[e] Department of Biophysical Chemistry, Umeå University, S-901 87 Umeå, Sweden

ARTICLE INFO

Article history:
Received 9 June 2008
Revised 15 August 2008
Available online 30 August 2008

Keywords:
Paramagnetic relaxation enhancement
Relaxation dispersion
Proton T_1
Nickel salt
Mixed solvents

ABSTRACT

Aqueous solutions of simple nickel(II) salts are a classical test case for theories of the paramagnetic relaxation enhancement (PRE) and its dependence on the magnetic field (nuclear magnetic relaxation dispersion, NMRD), going back to late fifties. We present here new experimental data, extending the NMRD range up to 21 T (900 MHz). In addition to salt solutions in (acidified) water, we have also measured on solutions containing glycerol. The aqueous solution data do not show any significant changes compared to the earlier experiments. The interpretation, based on the general ("slow-motion") theory is also similar to the earlier work from our laboratory. The NMRD-data in mixed solvents are qualitatively different, indicating that the glycerol not only changes the solution viscosity, but may also enter the first coordination sphere of the metal ion, resulting in lower symmetry complexes, characterized by non-vanishing averaged zero-field splitting. This hypothesis is corroborated by molecular dynamics simulations. A strategy appropriate for interpreting the NMRD-data for the chemically complicated systems of this type is proposed.

1. Introduction

Studies of proton spin-lattice relaxation rates as a function of the magnetic field (nuclear magnetic relaxation dispersion, NMRD) in aqueous solutions of paramagnetic complexes have been an active field of research for long time. The status of the field is described in recent books [1,2] and a review volume [3]. Investigations of this kind carry potentially a wealth of information on structure and dynamics of the species involved, provided that an appropriate model for the paramagnetic effects on the relaxation rate, denoted commonly as paramagnetic relaxation enhancement, PRE, is available. Modelling the PRE has long been recognized as difficult [4], but it seems that some of the fundamental problems have been solved. In a recent study, various models proposed in the literature were compared with each other [5] and it was demonstrated that two of the models agreed very closely, in spite of large differences in the mathematical treatment, which is highly encouraging.

Even the advanced physical models assume, inevitably, major simplification of the complicated reality of chemical systems. In this communication, we return to a very simple case of acidified aqueous solutions of the nickel ions, Ni(II). The system has been studied many times, beginning with the classical study by Morgan and Nolle [6], who found no field dependence for the proton spin-lattice relaxation time in the field range 0.05–1.4 T. Bloembergen and Morgan [7] explained this observation in terms of rapid electron spin relaxation, caused by fluctuations of the zero-field splitting, ZFS, originating from collisional distortions of the hydration sphere of the ion. In late eighties, we reported an investigation of low-pH aqueous solution of Ni(II) at a series of magnetic field up to 11.7 T [8] and interpreted the experimental data using a theoretical model of Westlund et al. [9]. The same data sets were re-interpreted by Svoboda et al. [10], using a slightly more sophisticated version of the theory. The experiments show that the PRE increases with increasing magnetic field in the high-field range. This is in agreement with theory which predicts, however, that the NMRD curve should reach a maximum and then turn down. In this work, we report an attempt to reach the maximum by extending the measurements to even higher magnetic field, 21.1 T (900 MHz ^{1}H resonance frequency). In addition, we have also measured the NMRD profiles for Ni(II) dissolved in a mixture of water and glycerol, deuterated in the chain. The effect of adding glycerol turned out to be quite complicated. This led us to detailed considerations of suitable strategies for fitting extended experimental NMRD-data sets. Moreover, we

* Corresponding author. Fax: +46 8 16 31 18.
E-mail address: jk@physc.su.se (J. Kowalewski).

1090-7807/$ - see front matter © 2008 Elsevier Inc. All rights reserved.
doi:10.1016/j.jmr.2008.08.011

found it motivated to complement the NMRD measurements by molecular dynamics (MD) simulations.

2. Materials and methods

Nickel(II) trifluoromethanesulfonate was prepared as follows. $Ni(OH)_2$ (purchased from Sigma–Aldrich) was dissolved in the aqueous pH 0.2 trifluoromethanesulfonic (triflic) acid, the pH was determined afterward to be 0.14. A concentration c_{Ni} = 0.0889 M in this stem solution was determined for Ni(II) ion using standard gravimetrical methods. Glycerol-(1,1,2,3,3-d_5) was obtained from Cambridge Isotope Laboratories and used without further purification. The solutions for NMR relaxation work were prepared as follows. Three different samples of nickel(II) trifluoromethanesulfonate containing 0, 4.1 and 6.7 M glycerol, equivalent to, respectively, 0%, 35% and 55% w/w, were prepared by weighing glycerol and adding the stem solution up to the desired volume and weighing again. The solutions were transferred to 3, 5 and 10 mm o.d. NMR tubes. The 10 mm samples were used in the field-cycling apparatus, 5 mm at 4.7 T and 3 mm at 9.4 and 14.1 T. The measurements at 21.1 T were carried out on a separately prepared solution, with a slightly different Ni(II) concentration but with the same solvent mixtures. The measurements at that field were performed on capillaries, immersed in 5 mm tubes filled with DMSO-d_6. The samples used for relaxation measurement are below denoted as "no-glycerol", "glycerol35%" and "glycerol55%".

The measurements at fields up to 0.94 T (40 MHz ^{1}H resonance frequency) were performed using the Stelar SPINMASTER FFC field-cycling relaxometer at the Magnetic Resonance Center (CERM) at the University of Florence. Measurements at high fields, 4.7, 9.4 and 21.1 T were performed on Bruker Advance spectrometers, while a Varian Inova was used at 14.1 T. Spin-lattice relaxation rates at high fields were measured using inversion-recovery technique. The major difficulty in these experiments is to avoid radiation damping, when using samples with close to 100 M proton solutions. At 4.7 – 14.1 T, this was achieved by making measurements with the decoupler channel on broadband probeheads optimized for larger sample diameters than used in our experiments. In some cases, the probeheads were in addition detuned to reduce the *Q*-values. The problem was of course most severe at the highest field (where a very high sensitivity cryo-probehead was used), but the problem was in that case solved by using a minute amount (2 μl) of the Ni(II) solutions. The temperature was in all cases controlled using the standard variable temperature equipment provided by the manufacturers. The spin-lattice relaxation rates were evaluated using the standard software provided by instrument manufacturers. The measurements at high fields were repeated at least three-times, the experimental uncertainties are estimated to be about 5%. Field-cycling measurements have accuracy of about 1%.

The paramagnetic relaxation enhancement was obtained by subtracting the diamagnetic rates, assumed to be independent of the magnetic field. With the high concentration of Ni(II) in the paramagnetic samples, the diamagnetic corrections were always less than 1% of the paramagnetic rates.

The paramagnetic relaxation enhancement arises through the so-called inner-sphere and outer-sphere mechanisms. The former refers to the contribution from protons residing in the first coordination sphere of the paramagnetic metal ion, the latter to protons outside of the first sphere. The inner-sphere PRE is often dominant. According to Luz and Meiboom [11], the inner-sphere PRE depends on the spin-lattice relaxation time of protons in the complex, T_{1M}, the exchange lifetime of the protons in the first coordination sphere, τ_M, and the mole fraction of ligand protons in the bound position, P_M:

$$PRE = T_{1\mathrm{para}}^{-1} - T_{1\mathrm{dia}}^{-1} = \frac{P_M}{T_{1M} + \tau_M} \quad (1)$$

If $\tau_M \ll T_{1M}$, the fast exchange conditions prevail and the PRE expression simplifies to P_M/T_{1M}. The PRE is thus a product of a molecular property, $1/T_{1M}$, and the molar ratio which, in turn, is proportional to the number of protons in the inner-sphere complex and to the concentration of the paramagnetic species.

As was discussed by Hertz the use of strongly acidified solutions and elevated temperatures (that is why we chose to work at 323 and 343 K) ascertains the fast exchange conditions [12]. The calculation of the mole fraction of bound protons is trivial for the solution without glycerol: $P_M = c_{Ni} \cdot q_H / 2c_{H_2O} = 9.70 \cdot 10^{-3}$, where q_H is the number of protons in the aqueous complex (equal to twelve), c_{H_2O} is the concentration of water (we set it to 55 M, neglecting the acid) and c_{Ni} = 0.0889 M. The same calculation requires a certain care in the mixed solvent cases. The molar concentrations of Ni(II), c_{Ni}, glycerol (c_{gly}) and water (c_{H2O}) are calculated from the known masses/volumes of the stem solution and the mixtures (see Table 1). We see in all cases only one proton signal arising from the water protons in fast exchange with the hydroxyl protons of glycerol. We consider thus the protons of these two kinds as a single pool. Every water molecule contributes two protons to that pool, while every glycerol contributes three protons from the hydroxyl groups. The expression for P_M thus becomes: $P_M = c_{Ni} \cdot q_H / (2c_{H_2O} + 3c_{gly})$. We assume that q_H = 11 in the glycerol-containing samples (see Section 3 below). This results in the P_M values in the "glycerol35%" and "glycerol55%" samples listed in Table 1.

The experimental in-complex relaxation rates, T_{1M}^{-1}, obtained from Eq. [1] are compared with calculations using the general "Swedish slow-motion theory" [13]. In order to perform least-squares fits of the parameters of the models to the experimental data, the slow-motion program was interfaced to the Minuit program package [14]. In order to estimate the possible outer-sphere contributions, we also report some calculations using the outer-sphere version of the theory [15].

Molecular dynamics (MD) simulations were carried out in an isothermal-isobaric, (*NPT*) ensemble at 298 K and atmospheric pressure. A solution of one Ni(II) ion among 100 glycerol and 340 water molecules, concentration about 60 weight per cent of glycerol, was simulated in a cubic cell with the periodic boundary conditions. The temperature was kept constant by using Nose–Hoover method [16,17], and the pressure by the Nose–Hoover barostat [18]. The equations of motion were solved using the double time step algorithm by Tuckerman et al. [18,19] with a long time step of 10 short time steps of 0.2 fs. The long-range Coulomb forces were calculated using the Ewald summation method.

Water is simulated with the flexible SPC-F model by Toukan and Rahman [20]. To describe glycerol molecules, the slightly modified version of Blieck et al. [21] potential based on the AMBER force-field, adopted by Chelli et al. [22], was used. In the present simulations, the value of atomic charge of the aliphatic hydrogen of central CH group was increased to 0.044 electronic units in order to bring the net molecule charge to zero. The stretching type potentials for C–H and O–H bonds, which are considered to be rigid in the original force-field, were added also. The corresponding force constants were taken from CHARMM22 force-field [23] which is

Table 1
Composition of the samples used in this study

Sample	c_{Ni}, M	c_{H2O}, M	c_{gly}, M	P_M
0% Glycerol	0.0889	55.0	—	$9.7 \cdot 10^{-3}$
35% Glycerol	0.063	40.9	4.1	$7.4 \cdot 10^{-3}$
55% Glycerol	0.046	29.6	6.7	$6.4 \cdot 10^{-3}$

based on high-level *ab initio* calculations. Ni(II)-water interactions were simulated with the potential proposed by Chillemi et al. [24]. To our knowledge, there is no potential especially adapted to describe Ni(II)–glycerol interactions available in the literature. In the present simulations the standard sum of Coulomb and Lennard–Jones 6–12 potentials was used. Two variants of Ni(II) Lennard–Jones parameters were considered: $\sigma_{Ni} = 2.050$ Å, $\varepsilon_{Ni} = 0.4184$ kJ/mol proposed by Wallen et al. [25], and $\sigma_{Ni} = 2.525$ Å, $\varepsilon_{Ni} = 0.0628$ kJ/mol by Rappe et al. [26]. Both variants, henceforth referred to as W-nickel [25] and R-nickel [26], respectively, were used in the simulations.

3. Results and discussion

The full set of experimental in-complex relaxation rates, T_{1M}^{-1}, is shown in Fig. 1. The results for the sample without glycerol are in very good agreement with earlier data [6,8]. At low field, we see practically no variation with either the magnetic field or temperature, while some variability can be seen in the high-field range. The results for the two glycerol-containing samples are characterized by qualitatively different NMRD profiles compared to the aqueous sample. Also in these cases, the profiles at low-field are flat and essentially temperature-independent, while the high-field data span much broader range of relaxation rates, in particular for the 55% glycerol sample. For all data sets, we can see that 21.1 T was not sufficiently high field to yield the expected turning point in the NMRD profiles. The physical origin of the maximum in the NMRD profiles is a combination of, on the one hand, an increase of the PRE caused by reduced effective electron spin relaxation rate at high-field and, on the other hand, a decrease of the electron spin–nuclear spin dipolar spectral density as the nuclear Larmor frequency goes up.

One of the goals of this study is to develop a suitable strategy for fitting a large data set of NMRD-data, including several solution compositions and temperatures. We have decided to treat each of the samples separately, but to try to fit the two-temperature data sets jointly, keeping as many parameters as possible temperature-independent.

Before going into the details of the fitting strategy, we wish to review briefly the model we use and its parameters [4,5,13]. The model assumes that the PRE is caused by the dipole–dipole (DD) interaction between the nuclear spin (I) and the electron spin (S). The strength of the DD interaction is inversely proportional to the third power of an effective distance between the spins, r_{IS}. The DD interaction is modulated by two processes: reorientation of the *IS* axis and electron spin relaxation. In principle, the chemical exchange could also be a modulation mechanism for the DD interaction, but we assume that it is much slower than reorientation and electron spin relaxation, at the same time as we consider the exchange to be very fast compared to nuclear spin relaxation. The reorientation process is considered as isotropic rotational diffusion in small steps, described by a rank–two rotational correlation time, τ_R. The electron spin relaxation is a complicated process, governed by the interplay of the Zeeman interaction and the zero-field splitting (ZFS) interaction. The ZFS interaction is a rank-two tensorial interaction, which is assumed to contain two components. The first one is "static" or "permanent" (in the same sense as molecules have a permanent dipole moment) and arises through averaging over fast motions (deformations of the complex by collisions and/or damped vibrations). Its principal axis system reorients with the molecule, in a similar way as the dipole–dipole axis. The static ZFS is assumed to be cylindrically symmetric and thus characterized by a single parameter, denoted D_S. In addition to that, we talk about a "transient" ZFS component, which can be thought of as a deviation of the instantaneous ZFS interaction from the static one. Also the transient ZFS is assumed to have cylindrical symmetry, with a single interaction strength parameter, D_T. The motion of the principal axis of the transient ZFS is also assumed to be possible to describe by isotropic rotational diffusion equation. This "pseudorotation" model [27] of the transient ZFS introduces thus a second dynamic parameter, a pseudorotational correlation time, τ_D. The pseudorotation model is a gross oversimplification of very complex dynamics [28,29], but seems to be able to capture the features which are most important for the PRE and its field dependence [30]. The problem of calculation of the PRE as a function of the magnetic field is complicated mainly for following reasons. (1) The ZFS is often so strong that the electron spin relaxation problem cannot be treated using perturbation theory (or Redfield theory [31]). (2) The processes of modulation of the DD interaction by reorientation and by electron relaxation are not statistically independent. (3) As we vary the magnetic field, the relative importance of the Zeeman and ZFS interaction changes. The Swedish slow-motion theory deals with the problem in frequency domain, by setting up and inverting a very big matrix representation of the relevant interactions and the rotational and distortional motions. As demonstrated recently [5], the method is numerically equivalent to the time-domain approaches proposed by Fries, Rast and coworkers [32,33] and by Westlund and Åman [34]. Summarizing the parameters of the model, we have to deal with three "interaction strength" parameters: r_{IS}, D_S and D_T, and two correla-

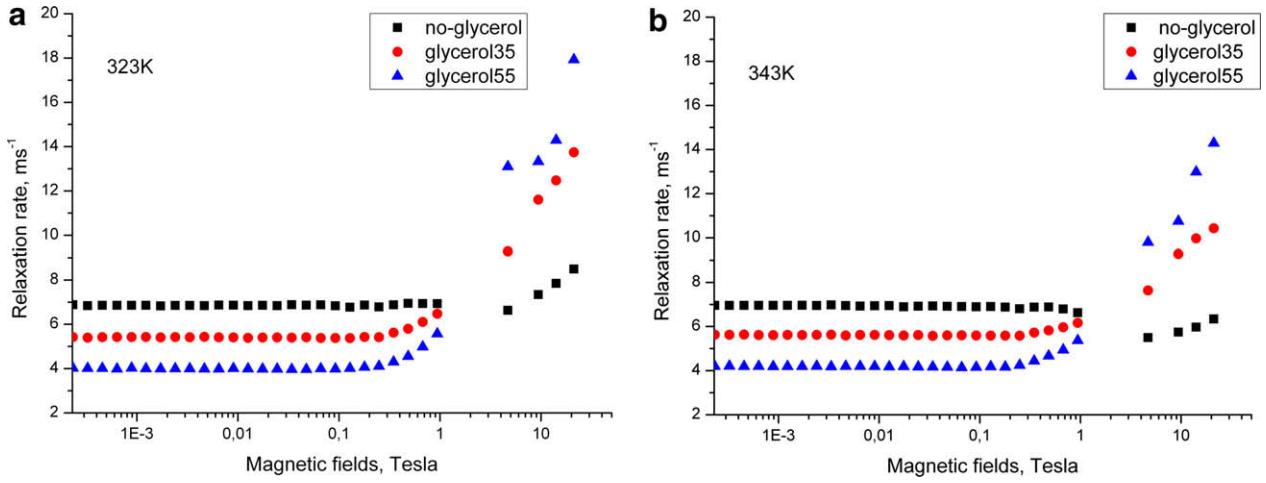

Fig. 1. Experimental NMRD profiles (in-complex relaxation rate, T_{1M}^{-1}, vs. magnetic field) for the three samples. (a) 323 K; (b) 343 K.

tion times, τ_R and τ_D. This number of parameters is much lower than the number of points in any of the NMRD profiles, but not obviously smaller than the number of distinct and characteristic features in a profile.

We begin the discussion with the "no-glycerol" sample. Qualitatively, the profiles at both temperatures are flat at low-field, up to about 1 Tesla, show a weak dip close to 5 Tesla and a weak increase above that field. Such features were noticed and explained in the early theoretical paper on the pseudorotation model by Westlund et al. [9]. We assume, in analogy with the earlier studies [8,10] that the static ZFS can be set to zero, because of the octahedral coordination (averaged on the time scale of molecular reorientation). In the earlier studies, the data at each temperature were fitted separately. Initially, we have done this also in the present case, but the fitted parameters obtained at the two temperatures turned out to be inconsistent with each other. Therefore we have decided, as a general strategy, to fit together the data sets at two temperatures (323, 343 K) for each sample. All interaction strength parameters are considered as temperature independent, while we use slightly different assumption concerning the temperature dependence of the correlation times for different samples. In the case of the "no-glycerol" sample, we allowed both the rotational correlation and the distortional correlation times to be different at the two temperatures. We performed the fits along two lines, which differed somewhat from each other. First, we adjusted parameters in groups, with the rotational correlation times, $\tau_R(323)$ and $\tau_R(343)$ in one group and the parameters related to transient ZFS, $\tau_D(323)$, $\tau_D(343)$ and D_T in the other. Parameters in each group were adjusted, together with the interspin distance r_{IS}, while the parameters in the other group were held fixed. This stepwise fitting was repeated until convergence and led to a very good agreement between calculations and experiments, displayed in Fig. 2a. The corresponding parameters are listed in Table 2. We have then tried a global least-squares fit of all six parameters together, *cf.* Table 2. The parameters changed in a non-negligible way, which we interpret as an indication of a certain numerical instability of the fitting strategy. The parameters obtained are quite reasonable. The nickel–proton distance is consistent with the X-ray structures of some Ni(II) salt hydrates, where the nickel–oxygen distance was reported as around 207 pm [35,36]. The comparison is based on the assumption that the electron spin can be treated as a point dipole [37], i.e. that the fitted distance corresponds to the nickel–hydrogen distance. The neutron diffraction data yield both the NiO (the same as X-rays) and the NiD distance (in the D_2O solution) of about 267 pm [38]. Enderby points out, however, that the measured NiD distance is a result of averaging over a wagging motion, characterized by a fairly broad distribution function [38]. The NiH distance obtained from EXAFS measurements was given as 277 pm [35].

The rotational correlation time attains a smaller value at a higher temperature as expected [39]. The values in Table 2 are in reasonable agreement with the value of rank-two rotational correlation time of 8 ps obtained for the HH vector in the first shell of the Ni^{2+} ion through MD simulations at 298 K [40]. Also the distortional correlation time shortens at higher temperature; here, however, it is difficult to say how reasonable this temperature variation is, since the pseudorotation model is a clear oversimplification of the physical reality [28,29]. Finally, the magnitude of the transient ZFS makes sense in comparison with estimates by Friedman et al. [41] and quantum chemical calculations [28].

Because of the instability of the fit and uncertain situation concerning the temperature variation of τ_D, we have also decided to perform least-squares fits with a temperature-independent distortional correlation time. Also the parameters resulting from this fit (denoted single τ_D) are shown in Table 2. The quality of the fit, measured by the target function (sum of squared errors, χ^2), becomes much worse, but the results are not dependent on the fitting procedure (stepwise or global). The agreement between the calculated and experimental NMRD profiles is still quite good, *cf.* Fig. 2b.

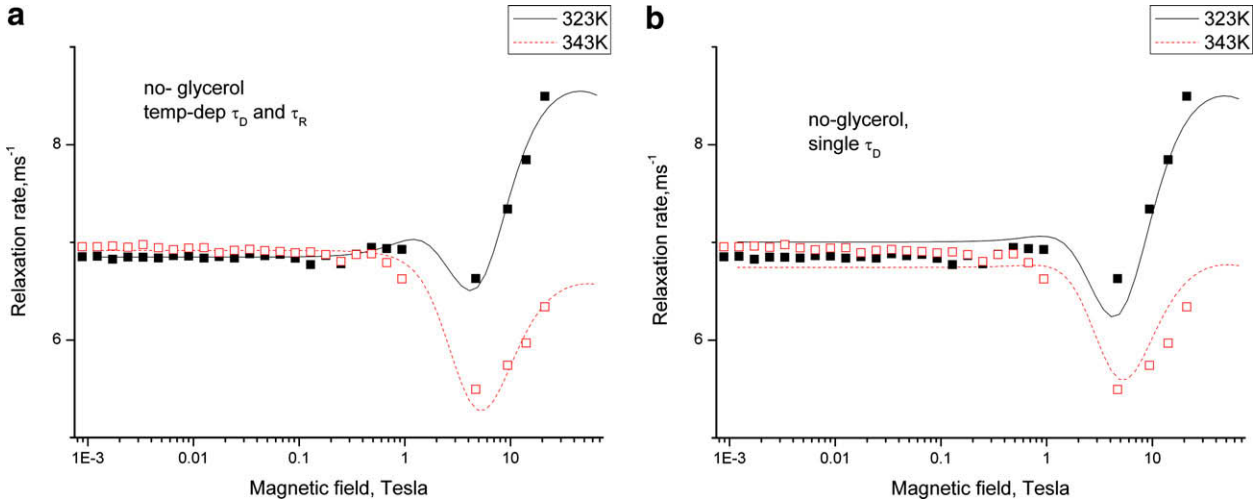

Fig. 2. Experimental and fitted NMRD profiles for the "no-glycerol" sample. (a) τ_D at each temperature adjusted separately (stepwise fit); (b) single τ_D, temperature-independent (stepwise fit). Corresponding parameters are listed in Table 2.

Table 2
Best-fit parameters for the "no-glycerol" sample

Fit	Distance, pm	$\tau_D(323)$, ps	$\tau_D(343)$, ps	$\tau_R(323)$, ps	τ_R (343), ps	D_T, cm^{-1}	χ^2
Stepwise	246	2.6	1.6	7.8	6.0	4.3	0.22
Global	240	2.3	1.3	6.8	5.2	5.1	0.18
Single τ_D, stepwise	246	2.0	2.0	7.7	6.1	4.3	1.97
Single τ_D, global	246	2.0	2.0	7.8	6.1	4.2	1.97

In the single distortional correlation time case, we have also performed fittings using a fixed NiH distance of 267 pm (from the neutron diffraction). The results obtained were unsatisfactory, in the sense that the resulting χ^2 was about 4.7, much higher than the other values in Table 2.

We then turn to the glycerol55% sample. Comparing the measurements on this sample with the "no-glycerol" results in Fig. 1 indicates a qualitative rather than quantitative difference. In fact, the NMRD profile for the glycerol55% sample reminds of the water proton profiles reported for Ni(II) complexes of symmetry lower than octahedral [42]. We tried nevertheless to fit the data using a similar approach as for the sample without glycerol (after some preliminary fitting attempts, performed in different ways, we realized that a large part of the target function came from the point 4.7 T and 323 K. This point was discarded in subsequent analysis). The T_{1M}^{-1} values used in the fitting were obtained using the P_M of Table 1, based on the assumption of $q_H = 11$. This q_H is more consistent with the discussion below, allowing for a glycerol molecule in the first coordination sphere, but we use it also in this first fitting approach in order to work with a single "experimental" set of T_{1M}^{-1} values. This analysis yielded a very long effective nickel–proton distance and a rather mediocre fit, *cf.* the first line Table 3 and Fig. 3a.

This led us to considering an alternative explanation, which might be that the dominant species at this solution composition is not a hexaaquo-Ni(II), but rather a species containing a glycerol molecule in the first coordination shell. The mixed water/glycerol solutions of Fe(III), Cr(III) and Mn(II) were studied earlier by Bertini et al. and their data indicated clearly the possibility of glycerol entering the first coordination sphere [43–45]. In order to investigate whether this was a reasonable possibility for Ni(II), we embarked on a series of molecular dynamics simulations (see Section 2 for details) starting with different possible structures of the Ni(II) coordination sphere, Fig. 4.

These configurations either appeared spontaneously during the preliminary MD runs or were manually constructed. The following equilibration procedure was performed for each of the latter structures. The complex was inserted into the manually created cavity in the periodic cell. The positions of all atoms in the complex were fixed during the 1 ns equilibration run. Thereafter, water molecules of the complex were allowed to move freely during the following 1 ns run. Finally, all the molecules in the complex were free to move and a complete simulation run was performed. The duration of simulation run varied from at least 5–10 ns.

Concerning ligand exchange processes, the species with five waters and one glycerol (the **5-1** structure) as well as hexaaquo-Ni(II), **6-0,** remained stable over the simulation time of 10 ns, while **4-2** and **3-1** complexes both did transform to **5-1** type structures. The stability of **4-1-13** (the notation means four waters and one glycerol in the first sphere, with the glycerol molecule acting as bidentate ligand, binding in the positions 1 and 3) and **4-1-23** complexes appears to depend on the type of Ni–glycerol potential employed. For R-nickel, the **4-1-13** complex remained stable over 5 ns simulation run whereas **4-1-23** transformed to **5-1** type structure. For W-nickel the situation changed: **4-1-23** complex remained stable over 5 ns whereas **4-1-13** transformed to **5-1** type structure. Thus, the MD simulations give at least some support to our hypothesis about the NMRD profile corresponding to a structure of lower symmetry, characterized by the presence of both a static and a transient ZFS.

In addition, MD simulations were performed within the expanded ensemble (MDEE) [46,47] in order to compute the free energy of solvation using both the Ni–glycerol interaction potentials (W and R). A 20 ns run was carried out in expanded space using the

Table 3
Best-fit parameters for the glycerol-containing samples, assuming single species

Sample/fit	Distance, pm	τ_D(323), ps	τ_D(343), ps	τ_R(323), ps	τ_R (343), ps	D_T, cm^{-1}	D_S, cm^{-1}	χ^2
Glycerol55%, single τ_D, no static ZFS	288	4.4	4.4	42	35	3.3	0	13.4
Glycerol55%, single τ_D, D_T locked	260	3.7	3.7	23	19	4.3[a]	5.7	6.8
Glycerol55%, single τ_D, global	256	3.4	3.4	22	18	4.8	6.1	6.5
Glycerol55%, T-dep. τ_D, stepwise	262	4.9	6.6	25	20	5.5	3.3	4.9
Glycerol55%, T-dep. τ_D, global	269	6.2	9.1	30	23	5.8	2.1	4.5
Glycerol35%, single τ_D	259	4.8	4.8	17	13	4.3[a]	2.6	1.2

[a] Locked in the fitting.

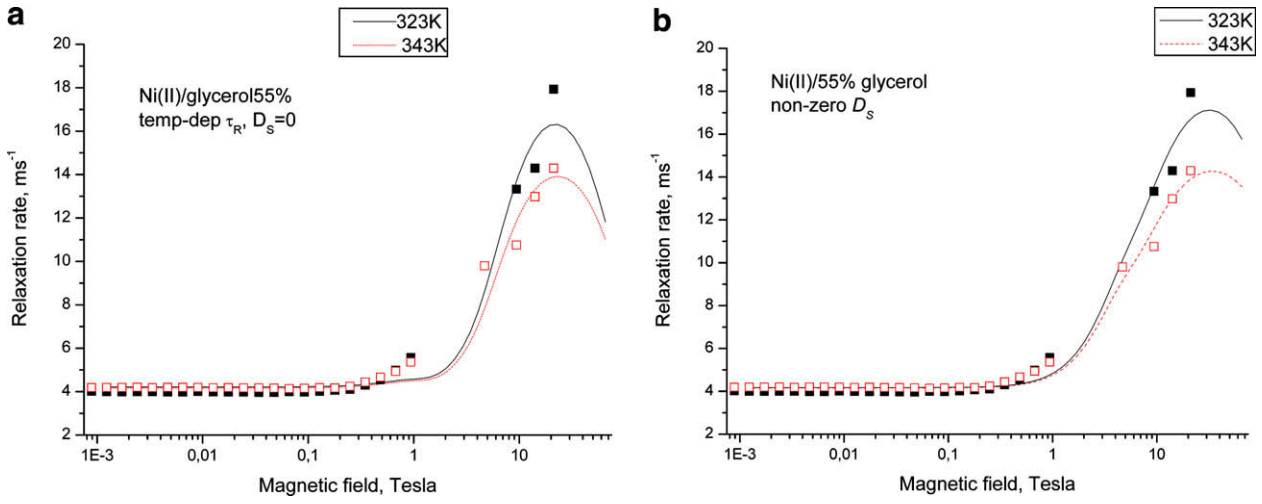

Fig. 3. Experimental and fitted NMRD profiles for the "glycerol55%" sample. (a) D_S fixed, equal to zero; (b) D_S adjusted, D_T fixed, single τ_D. Corresponding parameters are listed in Table 3, 2nd line.

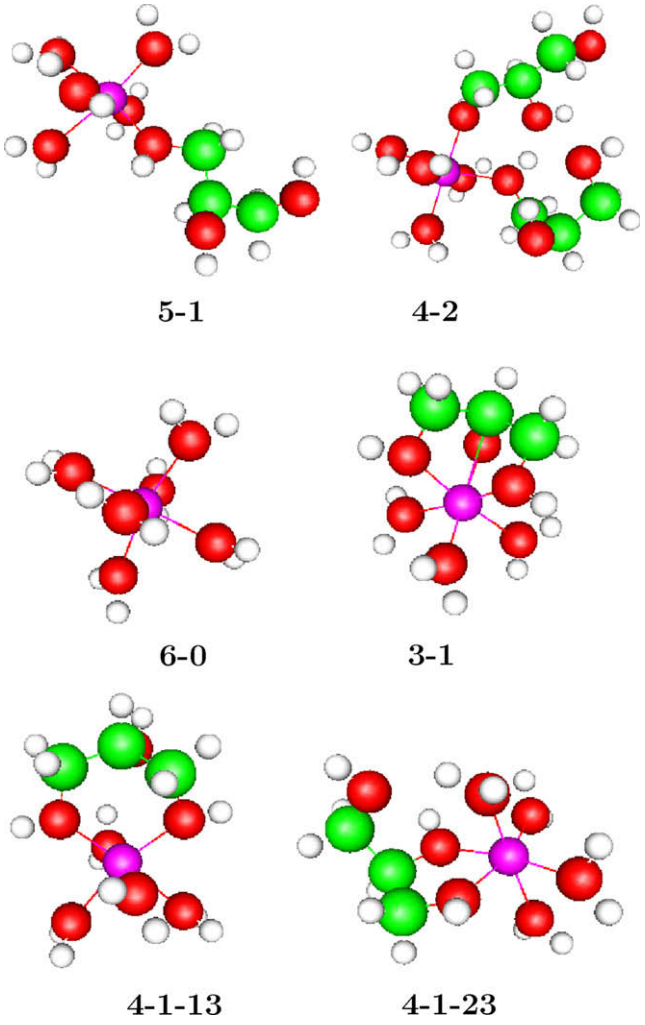

Fig. 4. Complex structures used as starting points for MD simulations.

R potential and starting the simulations from the **5-1** structure. Altogether 20 different configurations of the first coordinations sphere of the nickel ion were observed. Only in one case (in the beginning of the simulation) there was a preference of the initial complex structure, in all other cases the **6-0** was dominant. Using the W-model, 16 configurations were observed during the 20 ns run and all of them suggest the six-water structure as the most dominant configuration for the first coordination sphere around nickel. In principle, the computationally much more CPU-demanding MDEE method should give more reliable results but the number of configurations observed during the simulations is still rather limited, which makes it difficult to draw definite conclusions. In summary we can say that the **6-0** configuration has the highest preference but that there is still a finite probability to observe even **5-1** in light of both the standard MD simulations and the MDEE simulations. More studies with improved potential models as well as *ab initio* simulations may give more definitive answers to this question. Two additional pieces of information obtained from the MD simulations are of interest for the present study. First, the rank-two rotational correlation time for a water molecule in the **6-0** first shell of the nickel(II) ion in the mixed solvent at 298 K was in the range 80-86 ps, while the corresponding value for the **5-1** species was 62–69 ps. Second, the mean distance between the nickel ion and the exchangeable pool protons in the first shell, calculated as the sixth root of $1/\langle r^{-6}\rangle$, was 282 pm in the **6-0** and 305 pm in the **5-1** species, respectively. A more complete account of the MD simulations is beyond the scope of this paper and will be presented in a separate communication.

We moved then on to fitting the glycerol55% data without setting the static ZFS to zero. We began with assuming a single, temperature-independent distortional correlation time. In the first round, the parameters τ_D and D_T were also assumed to be the same as in the sample without glycerol, $\tau_D = 2$ ps and $D_T = 4.3$ cm^{-1}. In the second round we let one of these parameter to be adjusted, along with r_{IS}, D_S, $\tau_R(323)$ and $\tau_R(343)$. Locking $D_T = 4.3$ cm^{-1} gave the best fit and reasonable parameters, listed in the second line of Table 3. Then, we also performed a global fit with a single τ_D (*cf.* Table 3), which did not lead to very large changes. We can note that the metal–proton distance comes out in this case longer than for the pure aqueous sample. This is reasonable, as the proton pool now also contains the hydroxyl protons, at least some of which do not come very close to the nickel ion. Also, it is in agreement with the MD simulations. Another parameter with a clear physical significance is the rotational correlation time. According to the simple Stokes–Einstein–Debye theory, the correlation time is expected to be proportional to viscosity (η) divided by temperature. We plot the rotational correlation time (values corresponding to global fit with single τ_D) vs. η/T in Fig. 5 (we display in that graph the correlation times given in the 2nd line of Table 3). The resulting plot is reasonably linear. Moreover, the rotational correlation times in the Table are in decent agreement with the MD results, given the fact that these were obtained at lower temperature. The static ZFS turned out to be somewhat larger than its transient counterpart. The fitted single τ_D in the glycerol55% sample is larger than in the "no-glycerol" case, but we abstain from drawing any conclusions from this observation.

In the next step, we also allowed for the distortional correlation time to be dependent on the temperature, performing the fitting in a stepwise or global manner. In analogy to the "no-glycerol" data, the two fits differed in a non-negligible way. All the fitted parameters are shown in Table 3. We can note that fits with distinct $\tau_D(323)$ and $\tau_D(343)$ produced $\tau_D(343) > \tau_D(323)$. While this does not need to be unphysical, because of the oversimplified nature of the pseudorotation model (and while the uncertainties of the fitted parameters are certainly quite large), it strengthens our impression that, for the glycerol55% sample, it might be wisest to use a single τ_D value. The result of such a fit (corresponding to the 2nd line of Table 3) is displayed in Fig. 3b.

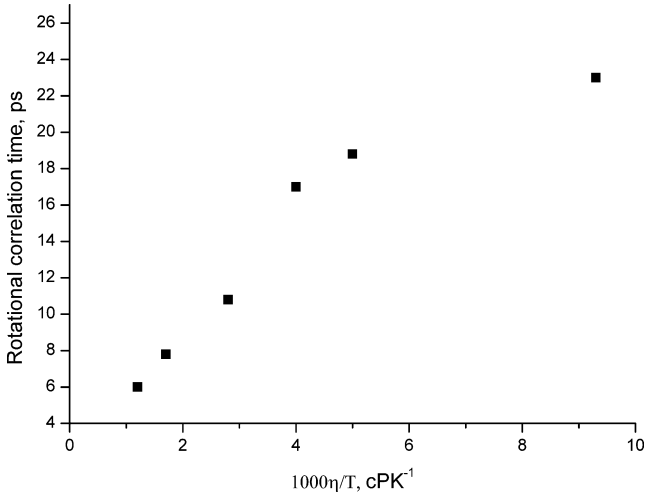

Fig. 5. Fitted rotational correlation times versus the viscosity divide by temperature for water–glycerol mixtures at 323 and 343 K. The viscosities were interpolated using the data from Landolt-Börnstein [48].

Before leaving the glycerol55% sample, we wish to mention another possible explanation of the change the NMRD profile (and in particular its low-field part) compared to the "no-glycerol" sample, not involving any lengthening of the NiH distance. In the system with low symmetry, such as our **5-1** species, the static ZFS does not need to be axially-symmetric. The presence of a static rhombic ZFS component, E_S, has a large effect on the low-field PRE for $S = 1$ [49–51]. The observed decrease of the low-field PRE upon adding glycerol might reflect this phenomenon. We have done some tests of this possibility but the results were inconclusive.

Finally, we turn to the glycerol35% data. We have in this case adopted two distinct strategies. Looking again at Fig. 1, we can see that the shapes of the NMRD profiles for the two glycerol-containing samples are quite similar. Therefore, one of the natural strategies for this sample might be analogous to what we did for the glycerol55% sample. In the last line of Table 3, we show the results obtained in this way, again locking the transient ZFS at $D_T = 4.3\ \mathrm{cm}^{-1}$ and fitting the r_{IS}, D_S, $\tau_R(323)$ and $\tau_R(343)$, as well as a single, temperature-independent τ_D. The fitted distance turns out be similar to the results for glycerol55%. The rotational correlation times follow, at least roughly, the viscosity changes also in this case, *cf.* Fig. 5. The static ZFS is smaller than what we have obtained for the glycerol55% sample. The best-fit NMRD profiles calculated in this way are compared with experimental data in Fig. 6a.

There is one problem with that fitting strategy: it assumes a single kind of paramagnetic species in solution. According to our MD simulations, we are not likely to have only low-symmetric complexes in solution. Therefore, we tried also another strategy: to fit the NMRD profile in term of two species in fast exchange with each other and with different populations. One of the species was assumed to retain the octahedral-symmetry around the Ni(II) ion, with vanishing static ZFS. The other one was assumed to be of lower symmetry, in analogy with the species assumed to dominate in the glycerol55% sample.

When trying to fit this model, we must be careful with the choice of parameters to be fitted. We decided to keep the number of fitted parameter at a minimum: four rotational correlation times (one for each of the two species at each of the two temperatures) and one of the populations at each temperature (the other population is obtained by subtracting the former from unity). All other parameters are assigned fixed values. The fixed and the adjusted parameters are collected in Table 4 and the calculated NMRD profile is shown in Fig. 6b. The rotational correlation times for the octahedral-symmetry species come out as somewhat shorter than for the low-symmetry complex at both temperatures. Both rotational correlation times decrease with increasing temperature. The populations at 343 K are closer to each other than at 323 K. All these findings make good sense. The quality of the fit is similar to that resulting from the single species assumption. One can of course ask the question whether the glycerol55% sample also corresponds to more than one species. The answer is that it very well might be so, but that we in that case do not really have another option than assuming a single species in the analysis.

All the analysis above was carried out assuming that all the measured PRE arises through the inner-sphere mechanism. This assumption can be validated *a posteriori* by estimating the outer-sphere contributions for the samples with the lowest viscosity (no-glycerol at 343 K) and with the highest viscosity (glycerol55% at 323 K) samples. We performed these calculations assuming that we deal with force-free diffusion in aqueous solutions, that the distance of closest approach is 350 pm and that the diffusion coefficients are proportional to the inverse viscosity. All other parameters are based on Tables 2 and 3. The results are that the maximum outer-sphere contribution would be 1.5% (the low viscosity case) or 3.5% (the high viscosity case), which validates the assumption that it could be neglected.

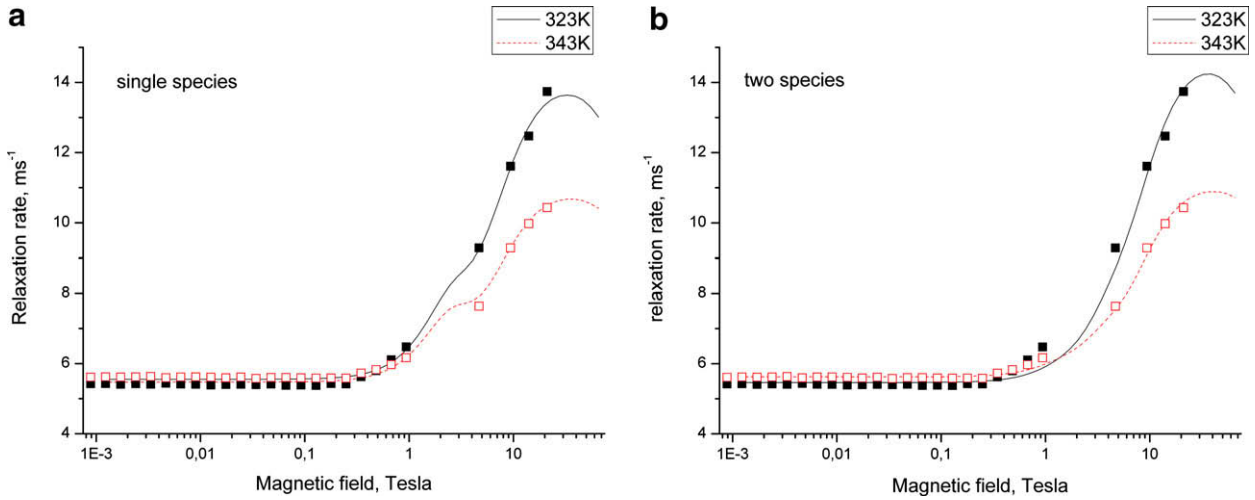

Fig. 6. Experimental and fitted NMRD profiles for the "glycerol35%" sample. (a) single species (parameters listed in Table 3, last line); (b) two species, parameters listed in Table 4.

Table 4
Best-fit parameters for the glycerol35% sample, assuming two species

Species	Distance, pm	D_S, cm^{-1}	$\tau_R(323)$, ps	τ_R (343), ps	Population (323)	Population (343)
1	246[a]	–	13	12	0.37	0.45
2	260[a]	5.7[a]	19	12	0.63	0.55

The parameters related to the transient ZFS were fixed throughout: $\tau_D = 3$ ps, $\Delta_T = 4.3\ \mathrm{cm}^{-1}$. The target function is 1.4.
[a] Locked in the fitting.

4. Concluding remarks

We present in this study an extensive set of multiple-field paramagnetic relaxation enhancement measurements for a nickel(II) salt solution in acidified water and in water–glycerol mixtures at two temperatures. The conditions are selected to ascertain that the fast exchange conditions pertain. The data are fitted using state-of-the art theoretical tools. Different strategies for parameter adjustment are compared to each other and discussed. In the "no-glycerol" sample, we deal with species with octahedral-symmetry, on average, with no permanent ZFS. The glycerol-containing samples display qualitatively different NMRD profiles, consistent with the presence of a species with the symmetry lower than octahedral and thus characterized by a permanent ZFS. It is also possible that more than one species is present in the glycerol-containing solutions. These findings are to a certain extent corroborated by molecular dynamics simulations. The parameters obtained in the fits are, by and large, very reasonable.

Acknowledgments

We are indebted to the CERM infrastructure access program (EUNMR, contract RII3-026145) for the generous grant of the instrument time on the field-cycling apparatus and on the 21.1 T spectrometer, as well as for the technical support. Valuable discussions with professor Claudio Luchinat are gratefully acknowledged. We thank professor Istvan Furo and Dr. Sergey Dvinskikh for access to, and assistance with the operation of, the 4.7 T spectrometer. This work was supported by the Swedish Research Council and by the Carl Trygger Foundation. A.V. Egorov gratefully acknowledges the Tokyo Boeki Scholarship and the Grants of the Russian Foundation for Basic Research (07-08-00548 and 07-03-00735).

References

[1] I. Bertini, C. Luchinat, G. Parigi, Solution NMR of Paramagnetic Molecules, Elsevier, Amsterdam, 2001.
[2] D. Kruk, Theory of Evolution and Relaxation of Multi-Spin Systems, Arima Publishing, Bury St. Edmunds, 2007.
[3] R. van Eldik, I. Bertini (Eds.), Advances in inorganic chemistry, Relaxometry of Water–Metal Ion Interactions, vol. 57, Elsevier, Amsterdam, 2005.
[4] J. Kowalewski, D. Kruk, G.G. Parigi, NMR relaxation in solution of paramagnetic complexes: recent theoretical progress for $S \geqslant 1$, Adv. Inorg. Chem. 57 (2005) 41–104.
[5] E. Belorizky, P.H. Fries, L. Helm, J. Kowalewski, D. Kruk, R.R. Sharp, P.-O. Westlund, Comparison of different methods for calculating the paramagnetic relaxation enhancement of nuclear spins as a function of the magnetic field, J. Chem. Phys. 128 (2008) 052315.
[6] L.O. Morgan, A.W. Nolle, Proton spin relaxation in aqueous solutions of paramagnetic Ions. II. Cr + + +, Mn + +, Ni + +, Cu + +, and Gd + + +, J. Chem. Phys. 31 (1959) 365–368.
[7] N. Bloembergen, L.O. Morgan, Proton relaxation times in paramagnetic solutions. Effects of electron spin relaxation, J. Chem. Phys. 34 (1961) 842–850.
[8] J. Kowalewski, T. Larsson, P.-O. Westlund, Proton spin-lattice relaxation in aqueous solution of the nickel(II) ion, J. Magn. Reson. 74 (1987) 56–65.
[9] P.-O. Westlund, N. Benetis, H. Wennerström, Paramagnetic proton nuclear magnetic relaxation in the Ni^{2+} hexaaquo complex. A theoretical study, Mol. Phys. 61 (1987) 177–194.
[10] J. Svoboda, T. Nilsson, J. Kowalewski, P.-O. Westlund, P.T. Larsson, Field-dependent proton NMR relaxation in aqueous solutions of Ni(II) ions. A new interpretation, J. Magn. Reson. A 121 (1996) 108–113.
[11] Z. Luz, S. Meiboom, Proton relaxation in dilute solutions of cobalt(II) and nickel(II) ions in methanol and the rate of methanol exchange of the solvation sphere, J. Chem. Phys. 40 (1964) 2686–2692.
[12] H.G. Hertz, M. Holz, Longitudinal proton relaxation rates in aqueous Ni^{2+} solutions as a function of the temperature, frequency, and pH value, J. Magn. Reson. 63 (1985) 64–73.
[13] T. Nilsson, J. Kowalewski, Slow-motion theory of nuclear spin relaxation in paramagnetic low- symmetry complexes: a generalization to high electron spin, J. Magn. Reson. 146 (2000) 345–358.
[14] MINUIT – Function Minimization and Error Analysis, CERN Program Library entry D506, CERN, Geneva, 1994–1998.
[15] D. Kruk, J. Kowalewski, to be published.
[16] S. Nose, A molecular dynamics method for simulations in the canonical ensemble, Mol. Phys. 52 (1984) 255–268.
[17] G.J. Martyna, D.J. Tobias, M.L. Klein, Constant pressure molecular dynamics algorithms, J. Chem. Phys. 101 (1994) 4177–4189.
[18] G.J. Martyna, M.E. Tuckerman, D.J. Tobias, M.L. Klein, Explicit reversible integrators for extended systems dynamics, Mol. Phys. 87 (1996) 1117–1157.
[19] M. Tuckerman, B.J. Berne, G.J. Martyna, Reversible multiple time scale molecular dynamics, J. Chem. Phys. 97 (1992) 1990–2001.
[20] K. Toukan, A. Rahman, Molecular-dynamics study of atomic motions in water, Phys. Rev. B 31 (1985) 2643–2648.
[21] J. Blieck, F. Affouard, P. Bordat, A. Lerbret, M. Descamps, Molecular dynamics simulations of glycerol glass-forming liquid, Chem. Phys. 317 (2005) 253–257.
[22] R. Chelli, P. Procacci, G. Cardini, S. Califano, Glycerol condensed phases. Part II. A molecular dynamics study of the conformational structure and hydrogen bonding, Phys. Chem. Chem. Phys. 1 (1999) 879–885.
[23] S. Reiling, M. Schlenkrich, J. Brickmann, Force field parameters for carbohydrates, J. Comput. Chem. 17 (1996) 450–468.
[24] G. Chillemi, P. D'Angelo, N.V. Pavel, N. Sanna, V. Barone, Development and validation of an integrated computational approach for the study of ionic species in solution by means of effective two-body potentials. The case of Zn^{2+}, Ni^{2+}, and Co^{2+} in aqueous solutions, J. Am. Chem. Soc. 124 (2002) 1968–1976.
[25] S.L. Wallen, B.J. Palmer, J.L. Fulton, The ion pairing and hydration structure of Ni^{2+} in supercritical water at 425° determined by X-ray absorption fine structure and molecular dynamics studies, J. Chem. Phys. 108 (1998) 4039–4046.
[26] A.K. Rappe, C.J. Casewit, K.S. Colwell, W.A. Goddard, W.M. Skiff, UFF, a full periodic table force field for molecular mechanics and molecular dynamics simulations, J. Am. Chem. Soc. 114 (1992) 10024–10035.
[27] M. Rubinstein, A. Baram, Z. Luz, Electronic and nuclear relaxation in solutions of transition metal ions with spin S = 3/2 and 5/2, Mol. Phys. 20 (1971) 67–80.
[28] M. Odelius, C. Ribbing, J. Kowalewski, Molecular dynamics simulation of the zero-field splitting fluctuations in aqueous Ni(II), J. Chem. Phys. 103 (1995) 1800–1811.
[29] M. Odelius, C. Ribbing, J. Kowalewski, Spin dynamics under the Hamiltonian varying with time in discrete steps: Molecular dynamics-based simulation of electron and nuclear spin relaxation in aqueous nickel(II), J. Chem. Phys. 104 (1996) 3181–3188.
[30] T. Larsson, P.-O. Westlund, J. Kowalewski, S.H. Koenig, Nuclear-spin relaxation in the slow-motion regime for the electron spin: The anisotropic pseudorotation model for S = 1 and the interpretation of nuclear magnetic relaxation dispersion results for a low-symmetry Ni(II) complex, J. Chem. Phys. 101 (1994) 1116–1128.
[31] A.G. Redfield, The theory of relaxation processes, Adv. Magn. Reson. 1 (1965) 1–32.
[32] S. Rast, P.H. Fries, E. Belorizky, Static zero field splitting effects on the electronic relaxation of paramagnetic metal ion complexes in solution, J. Chem. Phys. 113 (2000) 8724–8735.
[33] P.H. Fries, E. Belorizky, Relaxation theory of the electronic spin of a complexed paramagnetic metal ion in solution beyond the Redfield limit, J. Chem. Phys. 126 (2007) 204503.
[34] K. Åman, P.-O. Westlund, Direct calculation of ^1H_2O T_1 NMRD profiles and ESR lineshapes for the electron spin quantum numbers S = 1,3/2,2,5/2,3,7/2, based on the stochastic Liouville equation combined with Brownian dynamics simulation, Phys. Chem. Chem. Phys. 9 (2007) 691–700.
[35] P. D'Angelo, V. Barone, G. Chillemi, N. Sanna, W. Meyer-Klaucke, N.V. Pavel, Hydrogen and higher shell contributions in Zn^{2+}, Ni^{2+}, and Co^{2+} aqueous solutions: an X-ray absorption fine structure and molecular dynamics study, J. Am. Chem. Soc. 124 (2002) 1958–1967.
[36] Y. Marcus, Ionic radii in aqueous solutions, Chem. Rev. 88 (1988) 1475–1498.
[37] L. Nordenskiöld, A. Laaksonen, J. Kowalewski, Applicability of the Solomon–Bloembergen equation to the study of paramagnetic transition metal–water complexes. An ab initio SCF-MO study, J. Am. Chem. Soc. 104 (1982) 379–382.
[38] J.E. Enderby, Ion solvation via neutron scattering, Chem. Soc. Rev. 24 (1995) 159–168.
[39] J. Kowalewski, L. Mäler, Nuclear Spin Relaxation in Liquids, Taylor and Francis, New York, 2006.
[40] A.V. Egorov, A.V. Komolkin, A.P. Lyubartsev, A. Laaksonen, First and second hydration shell of Ni^{2+} studied by molecular dynamics simulations, Theor. Chem. Acc. 115 (2006) 170–176.
[41] H.L. Friedman, M. Holz, H.G. Hertz, EPR relaxation of aqueous Ni^{2+} ion, J. Chem. Phys. 70 (1979) 3369–3383.
[42] T. Nilsson, G. Parigi, J. Kowalewski, Experimental NMRD profiles for some low-symmetry Ni(II) complexes (S = 1) in solution and their interpretation using slow-motion theory, J. Phys. Chem. A 106 (2002) 4476–4488.
[43] I. Bertini, F. Briganti, Z. Xia, C. Luchinat, Nuclear magnetic relaxation dispersion studies of hexaaquo Mn(II) ions in water–glycerol mixtures, J. Magn. Reson. A 101 (1993) 198–201.
[44] I. Bertini, F. Capozzi, C. Luchinat, Z. Xia, Nuclear and electron relaxation of $Fe(OH_2)_6^{3+}$, J. Phys. Chem. 97 (1993) 1134–1137.
[45] I. Bertini, M. Fragai, C. Luchinat, G. Parigi, Solvent ^1H NMRD study of hexaaquochromium(III): inferences on hydration and electron relaxation, Inorg. Chem. 40 (2001) 4030–4035.

[46] A.P. Lyubartsev, A.A. Martsinovski, S.V. Shevkunov, P.N. Vorontsov-Velyaminov, New approach to Monte-Carlo calculation of free energy: method of expanded ensembles, J. Chem. Phys. 96 (1992) 1776–1783.
[47] A.P. Lyubartsev, A. Laaksonen, P.N. Vorontsov-Velyaminov, Free energy calculations for Lennard–Jones systems and water using the expanded ensemble method. A Monte Carlo and molecular dynamics stimution study, Mol. Phys. 82 (1994) 455–471.
[48] Landolt-Börnstein Zahlwerte und Funktionen, II. Band, 5. Teil, Bandteil a, Springer, Berlin, 1969.
[49] R.R. Sharp, Nuclear spin relaxation due to paramagnetic species in solution: effect of anisotropy in the zero-field splitting tensor, J. Chem. Phys. 98 (1993) 6092–6101.
[50] T. Nilsson, J. Svoboda, P.-O. Westlund, J. Kowalewski, Slow-motion theory of nuclear spin relaxation in paramagnetic complexes of arbitrary symmetry, J. Chem. Phys. 109 (1998) 6364–6375.
[51] I. Bertini, J. Kowalewski, C. Luchinat, T. Nilsson, G. Parigi, Nuclear spin relaxation in paramagnetic complexes of S = 1: electron spin relaxation effects, J. Chem. Phys. 111 (1999) 5795–5807.